Int. J. Electrochem. Sci., 16 **(2021)** Article Number: 21112, doi: 10.20964/2021.11.19

International Journal of
ELECTROCHEMICAL
SCIENCE
www.electrochemsci.org

Preparation of Electroless Copper Circuit on Polycarbonate/ Acrylonitrile Butadiene Styrene (PC/ABS) Using a Laser curing of Pd complex

Yi-Shin Chen[1], *Chih-Chia Wang*[2], *Jhu-Lin You*[2], *Chang-Pin Chang*[2,*], *Bo-Wei Lai*[2], *Ming-Der Ger*[2,*]

[1] School of Defense Science, Chung Cheng Institute of Technology, National Defense University, Taiwan 335, ROC
[2] Department of Chemical & Materials Engineering, Chung Cheng Institute of Technology, National Defense University, Taiwan 335, ROC
[*]E-mail: mingderger@gmail.com (M.-D. Ger), cpchang1@ndu.edu.tw (C.-P. Chang)

Received: 2 May 2021 / *Accepted:* 5 July 2021 / *Published:* 10 October 2021

A laser selective metallization on polycarbonate/acrylonitrile butadiene styrene (PC/ABS) substrates has been developed to fabricate copper patterns in this research. A laser curable Pd complex consists of 4-Vinylpridine (4VP), trimethylolpropanetriacrylate (TMPTA), tert-butyl peroxybenzoate (TBPB) and $Pd(OAc)_2$, is utilized. First, liquid-phase palladium complex deposited on flexible substrates is irradiated by the laser beam. This produced a cured Pd complex with an effective catalytic activity. Then, a copper layer can be selectively deposited in the laser activation area on the PC/ABS substrate to form a copper pattern with excellent adhesion by electroless deposition (ELD). Various laser curing parameters, including laser mode (continuous or pulsed), laser energy and laser wavelength, are investigated to elucidate their effects on the morphology of copper pattern and the adhesion between the copper layer and PC/ABS substrate. The copper coating plated in this way shows low resistivity, which can make the bulb bright and not peel off after testing the adhesion with 3M 600 tape. Moreover, we also demonstrate that the copper patterns can be prepared easily by laser-curing catalyst pattern, with electroless copper deposition, which is a fast and effective strategy for fabricating circuit patterns on the PC/ABS substrate.

Keywords: laser direct writing, catalytic ink, metal deposition, Copper circuit, PC/ABS

1. INTRODUCTION

Flexible electronics with thin and light features are used in wearable electronic equipments, portable apparatuses and radio frequency identification (RFID) devices and make related products more convenient for current demands [1-6]. One of the new methods for manufacturing flexible electronic products is to prepare metal line patterns on polymer layers. PC/ABS is an appropriate composite material with the respective characteristics. PC/ABS metallization has stimulated research along with

demands for embedded antennas in rapidly evolving wireless communication systems. Previous studies have reported that laser direct structuring (LDS) for PC/ABS is one of the most prevalent metallization methods [7-9]. LDS is a process of using laser for electroless plating areas on commercial polymers [10, 11]. Copper is one of the exceptional conductive metals for use in flexible electronics. Nowadays, the photolithography has been well applied to the manufacture of metallic patterns. However, there are still some problems, such as complicated steps, high cost and low yield in the techniques [12]. Shadow mask patterning sometimes results in insufficient resolution.

Rapid utilization of electroless deposition (ELD) to manufacture integrated circuits and interconnects for electronic devices results from its many advantages, such as reasonable process temperature, low cost of processing and compatibility [13-17]. Catalysts such as palladium (Pd) colloids or Pd(II) salts have been widely used to initiate the activity of metal deposits in various ELD solutions [18-20]. It has been reported that electroless plating of metal on the catalytic sites of polymer which was activated by printing catalytic ink onto the designed positions can effectively enhance the resolution of metallic patterns [15, 21-24] . In order to prevent deposited metal flaking, increasing surface roughness or changing surface function is usually utilized to enhance the adhesion between metal and polymer substrate. Laser patterning, a non-contact and maskless fabrication technique, is more economical and efficient than other patterning methods [25] such as microcontact printing [26, 27], screen printing [28] and inkjet printing [29-31]. The metallic patterns are related to the activated location of catalysis and the desired metallic patterns are obtained by the above procedures. Even though the laser patterning method tends to be more mature in recent years, the surface integrity of metal curing on substrates still needs to be greatly investigated and improved due to lack of effective complex catalyst and the basic parameters of appropriate laser energy for laser curing . Applying excessive pulse energy to laser curing of Pd complex catalyst will not only damage the surface of the material, but also reduce the adhesion between metal layer and polymer substrate . Some studies have shown that substrates are overheated with ease due to inappropriate use of laser energy, causing damage to its surface and reducing mechanical properties[32-35]. Other studies even have indicated that the laser curing process must be cautiously adjusted to obtain a better metal plating effect, but the process is cumbersome and inefficient[35-38].

In our previous study [39], a laser curable Pd complex ink consists of Pd salt, pH sensitive monomer N, N-dimethyl-dimethylaminoethyl methacrylate (DMAEMA), trimethylolpropane triacrylate (TMPTA), and tert-butyl peroxybenzoate (TBPB) is successfully used for selective metallization of polyimide (PI) substrate. However, the laser parameters effects have not been investigated. Different laser parameters not only lead to diverse catalytic activities and different substrate heating environments [35, 36], but also influence the electroless plating of copper deposit [20] . Moreover, the line width of the pattern is affected by laser energy due to the different extended widths caused by the heat accumulation effect. It has been reported that 4-vinylpyridine (4VP) is able to complex metallic palladium ions which then serve as catalyst for a copper electroless plating [40] . Thus, in this study, a similar Pd complex consisted of 4-vinylpridine (4VP), trimethylolpropane triacrylate (TMPTA) and tert-butyl peroxybenzoate (TBPB) was prepared which used 4VP instead of DMAEMA. This Pd complex was spin coated on the PC/ABS firstly. Then, the laser irradiation was utilized to effectively cure and reduce the Pd complex on the PC/ABS substrate. Finally, the copper layer can be selectively deposited in the laser activation area on the PC/ABS substrate to form a copper pattern by electroless deposition

(ELD). Laser wavelength, generated power and mode of operation (pulsed or continuous) have a significant influence on the surface properties of laser irradiated polymer material. The effects of laser parameters (frequency and duty cycle) on the morphology of the electrolessly plated copper layer are investigated.

2. EXPERIMENTS

2.1. Synthesis of laser curable Pd complex ink

All chemicals used in this work were reagent grade and acquired from Showa chemical. To enhance the adhesion strength between the copper film and PC/ABS substrate, a Pd complex based on $Pd(OAc)_2$, 4VP, TMPTA and TBPB was developed in this study. The synthesis of laser curable Pd complex is shown schematically in figure 1(A). First of all, 9.6×10^{-2} mol/L of 4-vinylpridine (4VP) monomer and 8.4×10^{-2} mol/L of trimethylolpropanetriacrylate (TMPTA) were added to ethanol. Secondly, 600 ppm of palladium acetate was dissolved in the aforementioned solution and sonicated for 10 min. After that, the peroxide tert-butyl peroxybenzoate (TBPB) was added to the solution to form the laser curable Pd complex. The effects of laser power density on the adhesion strength between the copper coating and the PC/ABS substrate were investigated stepwisely. Structural changes of Pd complex after laser irradiation were analyzed by FTIR-ATR spectroscopy. The surface cleaning and modification of PC/ABS was done using a base solution treatment and then a layer of $Pd(OAc)_2$ was coated onto the PC/ABS. X-ray photoelectron spectroscopy (XPS) was utilized to verify the reduction of the Pd ions by laser heating.

2.2. Polycarbonate/Acrylonitrile Butadiene Styrene surface modification

First of all, the PC/ABS substrates were hydrolyzed with 0.1M sodium hydroxide (NaOH) in an ultrasonic cleaner for 30 mins, then rinsed in deionized water (DI water) to clean excess NaOH solutions on the substrate. Finally, the modified PC/ABS substrates were dried in an oven to remove DI water completely.

2.3. Laser curing and electroless copper plating on Polycarbonate/Acrylonitrile Butadiene Styrene substrate

The processes of laser curing and electroless plating of Cu on PC/ABS are shown schematically in Figure 1 (B). For the lasering process, catalytic Pd complex was in advance coated on the PC/ABS film. The coated film was completely air-dried. A pulsed laser with a wavelength of 1064 nm (Taiwan Easylight Technology Co., Ltd.) was used for selective curing of Pd complex to form a desired Pd pattern. A beam expander and a microscope were used to focus the laser beam on the surface of PC/ABS substrate. The laser beam was focused into a spot with a size of less than 18 micrometers. In the study, laser light parameters such as laser power must be suitably controlled to achieve the desired heating effect. An unsuitable laser energy density change might result in an incorrect result. Fig.1 presents the schematic illustration of the heat-induce metal circuit fabrication process.

Based on the above experimental results, the subsequent experiment will cross-test the adjustment frequency with the duty cycle under the condition of suitable input energy. It is crucial to control the pulse intensity because the higher pulse intensity can produce a higher temperature during the laser processing. The single-shot pulse intensity (J) is the average power (W) divided by the frequency (number of times, F) and the pulse width (time, T). The single-shot pulse intensity (J) divided by the spot area is presented in the form of pulse energy density.

$$W / (F * T) = J$$

After the laser-direct writing process was completed, the PC/ABS surface was washed with DI water to remove the Pd ions and uncured monomers. Finally, the samples were immersed into the electroless plating bath for Cu deposition. The ELD of Cu was performed in a plating bath consisting of a 1:1 mixture of freshly prepared solutions A and B. Solution A contains NaOH (12 g/L), $CuSO_4 \cdot 5H_2O$ (13 g/L) and potassium sodium tartrate ($KNaC_4H_4O_6 \cdot 4H_2O$, 29 g/L) in DI water. Solution B is a 37 wt% HCHO (9.5 mL/L) aqueous solution. The electroless deposition was carried out at 50℃ to 65 ℃ and pH of 12.5 for 10 to 40 min, the stirring rate was 250 rpm. In this experiment, the heat is generated by the absorption of the laser wavelength on the substrate via utilizing the laser beam which is focused on the surface of the substrate, causing breakage of O-O bond to facilitate free radical polymerization. Palladium acetate is thermally cracked and reduced to palladium metal by the aforementioned heat as well. However, power, frequency, pulse width and scanning rate will all affect the thermal accumulation since the laser machine which we used is a pulsed laser.

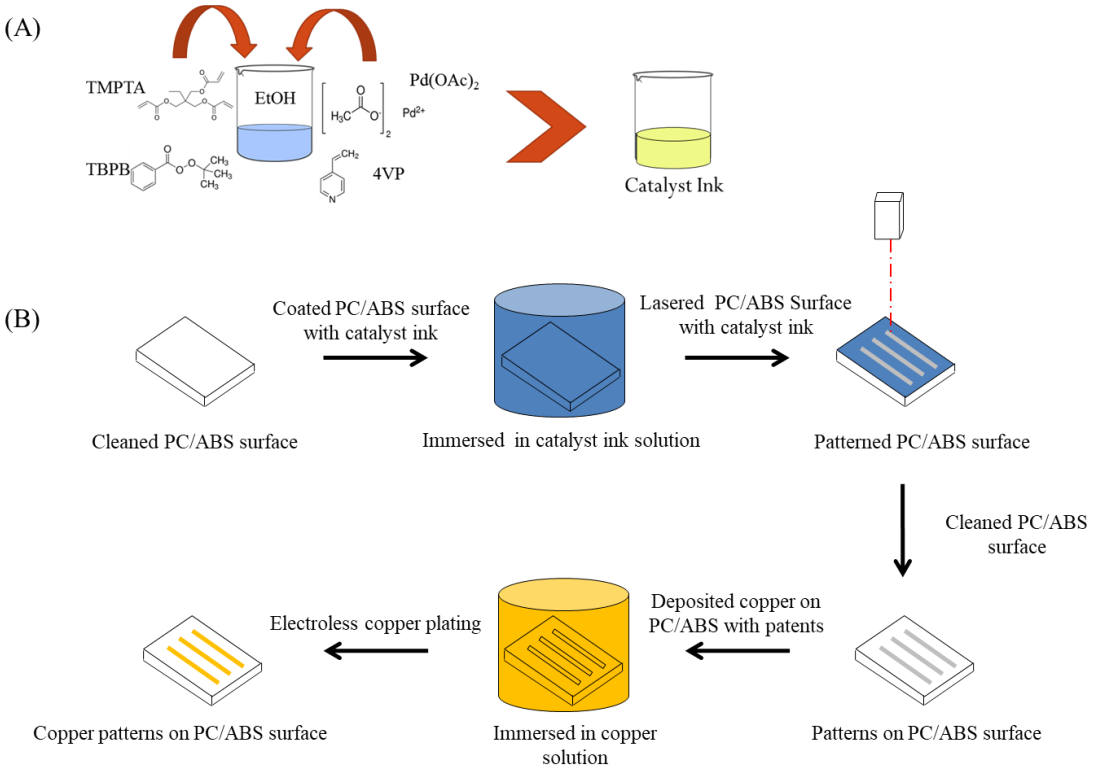

Figure 1. A schematic diagram showing (A) the preparation of catalytic Pd complex, (B) the fabrication process of Cu pattern on Polycarbonate/Acrylonitrile Butadiene Styrene substrates by integration of laser heating of Pd complex and electroless plating.

2.4. Characterizations

The FTIR analysis was carried out using a BRUKER TENSOR 37 FTIR-ATR spectrometer. The FTIR spectra were recorded in a wavenumber range of 4000–600 cm^{-1} with 64 scanning. Surface morphology and chemical composition were studied by field emission scanning electron microscopy (FE-SEM, S-3000N, HITACHI, Japan). The chemical structure of the modified substrates was measured by X-ray photoelectron spectroscopy (XPS, VG Micro Lab 310D, United States) using the monochromatized Al Kα line at 1487.6 eV. Electrical resistivity (in Ω/cm) of laser metal deposition before and after bending test were measured by Four-Point Probe (Keithley 2400, United States). According to ASTM D-3359, the adhesion between the metal pattern and the substrate was evaluated by using the 3M #600 tape test.

3. RESULTS AND DISCUSSION

3.1. Properties analysis of 4VP thermal cross-linking Pd complex

Palladium acetate, a catalyst, plays a pivotal role in laser cross-linking Pd complex [39]. Therefore, it is very important to study the phase changes of palladium acetate at different temperatures because of high temperature caused by laser energy on the substrate surface. The thermal properties of palladium acetate were detected by TGA as shown in Fig. 2. First of all, at about 220°C, it can be observed that the thermal cracking and vaporization of acetate causes a rapid decrease in weight percentage. The molecular weight of Palladium acetate is 224.5 g/mol, the molecular weight of Palladium is 106.42 g/mol, accounting for 47% in weight of Palladium acetate.

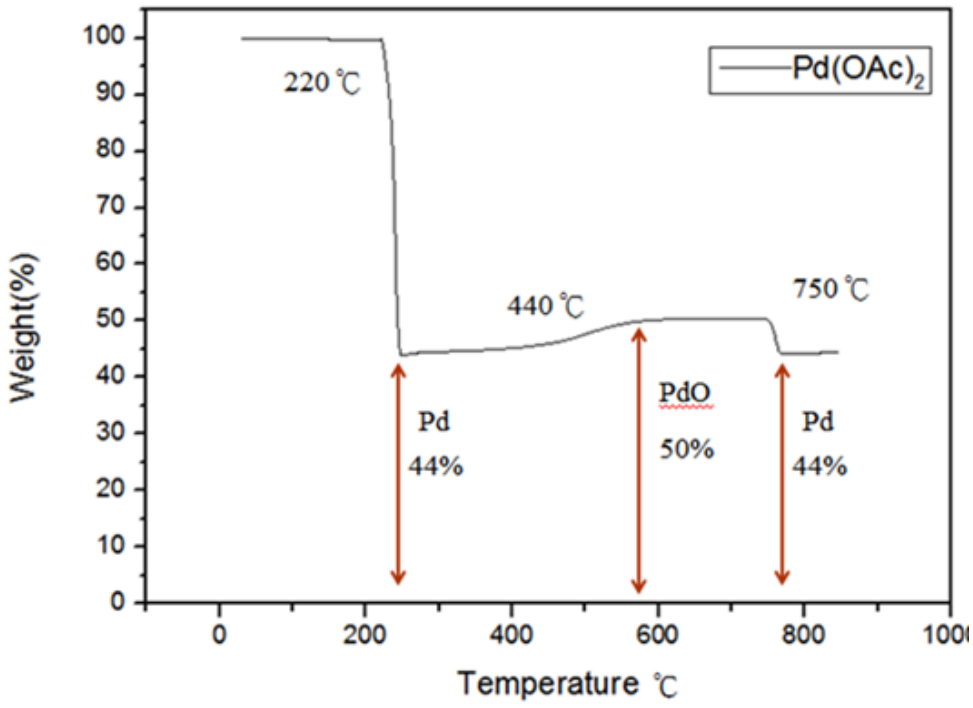

Figure 2. TGA pattern of Palladium acetate

When the temperature is raised to about 220°C, the remaining Palladium weight percentage in Palladium acetate is about 44%, which means that Palladium acetate can be decomposed and reduced to Palladium metal state. Next, above 440°C, Palladium metal becomes oxidized to produce Palladium oxide, which causes the weight percentage to rise. As the temperature is between 570°C and 750°C, the remaining percentage is about 50%, which means that the Palladium metal is oxidized at high temperature to produce Palladium oxide obviously. Finally, if the temperature continues to be raised above 750°C, the Palladium oxide will be heated and reduced to the Palladium metal state, reducing the weight percentage again to 44%. In addition, Palladium acetate produces an exothermic peak at 205°C in DSC, which corresponds to the weight loss of Palladium acetate at 220°C in the TGA analysis, shown in Fig. 3.

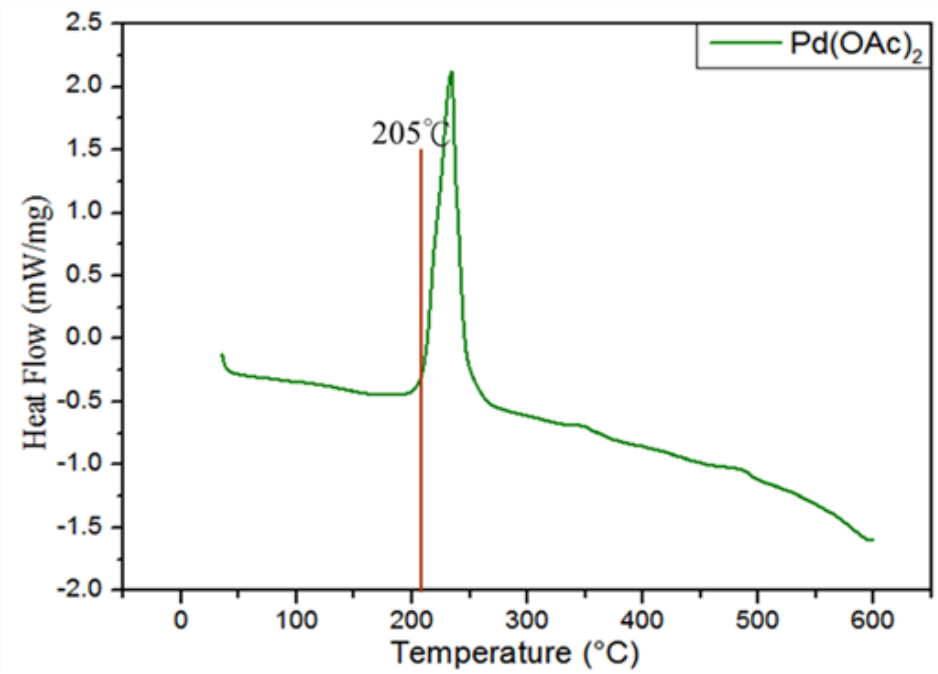

Figure 3. DSC pattern of Palladium acetate

The FTIR-ATR spectrum of Pd-based complex before and after laser irradiation is displayed, respectively, in Fig.4. The results are consistent with the literature in response to thermal cross-linking [39]. It is clearly observed that the presence of absorption characteristic peak at 1625 cm^{-1}, which is attributed to the C=C stretching vibration of 4VP and TMPTA, for the pristine Pd complex. In contrast, the characteristic peak at 1625 cm^{-1} is absent after laser heating, which suggests the successful polymerization and cross-linking of TMPTA and 4VP monomers.

XPS analysis was carried out to evaluate the state of palladium after laser heating. In total, four peaks were exhibited at 335.69, 337.98, 340.70 and 343.22 eV of the Pd XPS spectrum, as shown in Figure 5. The electron binding energy signal peaks at 343.22 eV and 337.98 eV were attributed to Pd^{2+} and the electron binding energy signal peaks at 340.70 eV and 335.69 eV was from of Pd^{0}. It indicates that Palladium acetate is reduced to palladium by laser heating. Based on the integral area, palladium

accounts for about 68% and palladium ions account for about32%. It can be clearly observed that both palladium species（ Pd^0, Pd^{2+} ）are located on the PC/ABS surface, depending on the laser heating [39].

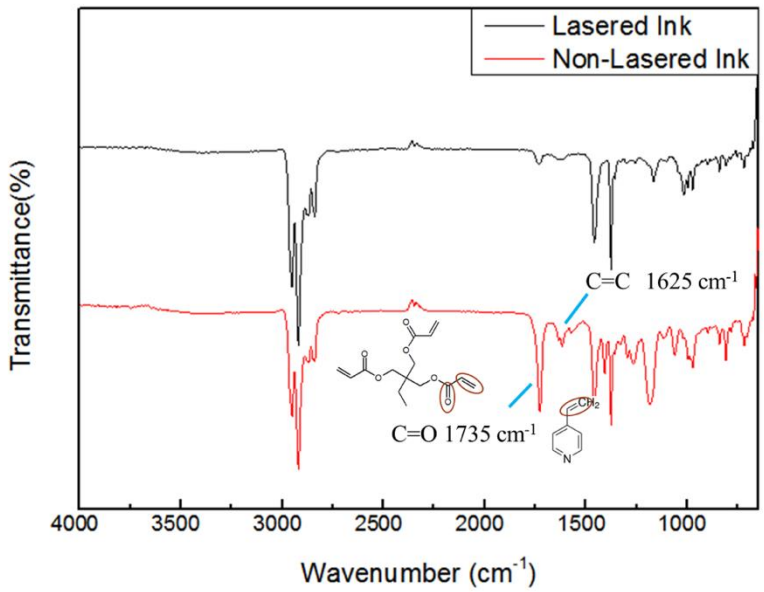

Figure 4. FTIR-ATR spectra of catalyst ink before and after laser.

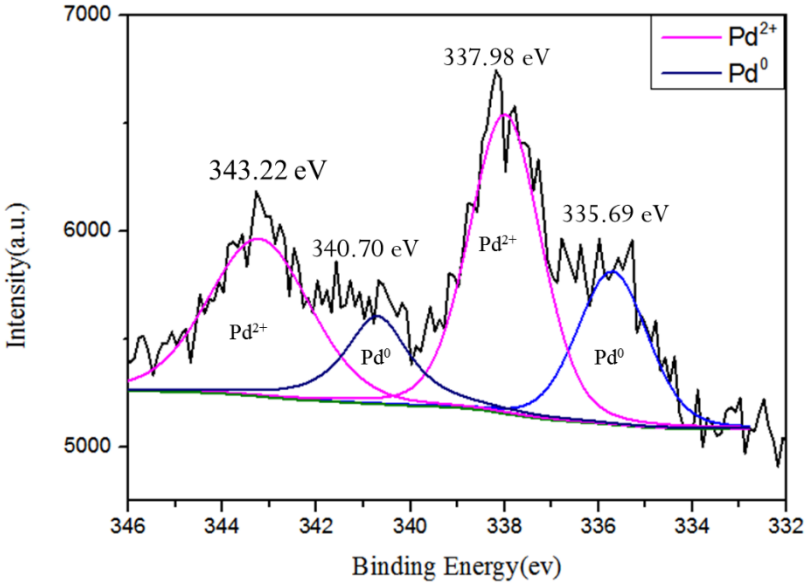

Figure 5. XPS Pd spectrum of $Pd(OAc)_2$ coated PC/ABS after laser heating.

3.2. Effect of laser parameters

In order to find the best cross-linking conditions for thermal cross-linking Pd complex with PC/ABS substrate and the optimal requirements for the reduction by the catalyst, we tend to employ different cross-tests on the aforementioned conditions to obtain the optimal laser parameters (Fig.6). The

power meter is used to measure the pulse energy density of each frequency and then the process of electroless copper plating is used to observe whether there is a copper deposit on the surface with SEM.

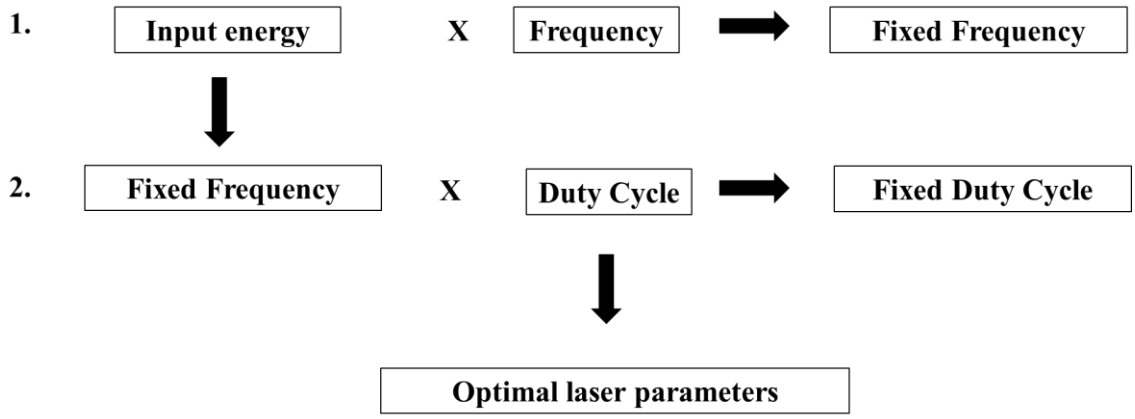

Figure 6. The diagram of laser parameter experiments framework

3.2.1. The effect of different laser frequencies on the electroless copper pattern

The pulse energy density depends on diverse frequencies [35]. Table 1 shows the variation of pulse energy density with fixed input energy of 10 %, duty cycle 40 % and frequency 20~90 kHz. As shown in Fig.7 (A)-(H), the surface of the pattern is observed by SEM after electroless deposition of copper. After the laser focusing mirror is focused, the spot diameter is about 18 μm. The output power is divided by the spot area and the energy density is presented. The parameter of Fig. 7(A) is frequency 20 kHz and power density is 87 μJ/μm^2. It can be seen that the PC/ABS is left with shallow traces on the surface after being scanned by the laser. However, the copper metal cannot be deposited after the plating, indicating that the increased temperature of this parameter is not enough to reach the temperature for reducing the catalytic ions. The parameters are 30 kHz and the power density is 197 μJ/μm^2 in Fig.7(B). It can be seen from the figure that there is a small amount of copper metal deposition on the line after the plating. However, the metal line cannot be continuous due to insufficient catalyst reduction because the number of laser scanning repetitions (frequency) and energy density increase contribute to heat accumulation. The area of copper metal deposition is more visible in Fig.7 (B), indicating that the proportion of catalyst reduction becomes higher, resulting in copper metal deposited on the pattern. It is better than Fig.7 (A). Fig.7 (C) has a frequency of 40 kHz and 30 kHz of Fig.7 (B), the increase in the number of laser scanning repetitions (ie, frequency) contributes to heat accumulation. It can be seen in Fig.7 (C) that the area of copper metal deposition is more than that of Fig.7 (B), indicating that the proportion of catalyst reduction is high, so that the copper metal deposited on the pattern is relatively complete. At Fig.7 (D)-(F), increase with frequency and energy density, the heat accumulating effect causes the increase temperature to reach the temperature required for catalytic ion reduction and the frequency rise makes the pattern more continuous. However, Fig.7 (G)-(H) show that when the number of laser scanning repetitions (frequency) is too large and the energy density is too large, the heat accumulation effect is too large, so that the catalytic activity is lowered and aging and the optimum

reaction temperature is missed, resulting in the pattern becoming discontinuous. According to these experimental data, it's needed to check the fixed frequency and different duty cycle. It is crucial to control the pulse intensity by duty cycle because higher pulse intensity can produce higher temperatures during laser processing.

Table 1. The pulse energy density on the duty cycle 40% at different frequencies (20 to 90 kHz)

Frequency (kHz)	Pulse energy density ($\mu J/\mu m^2$)
20 kHz	87 $\mu J/\mu m^2$
30 kHz	197 $\mu J/\mu m^2$
40 kHz	350 $\mu J/\mu m^2$
50 kHz	546 $\mu J/\mu m^2$
60 kHz	786 $\mu J/\mu m^2$
70 kHz	1071 $\mu J/\mu m^2$
80 kHz	1399 $\mu J/\mu m^2$
90 kHz	1770 $\mu J/\mu m^2$

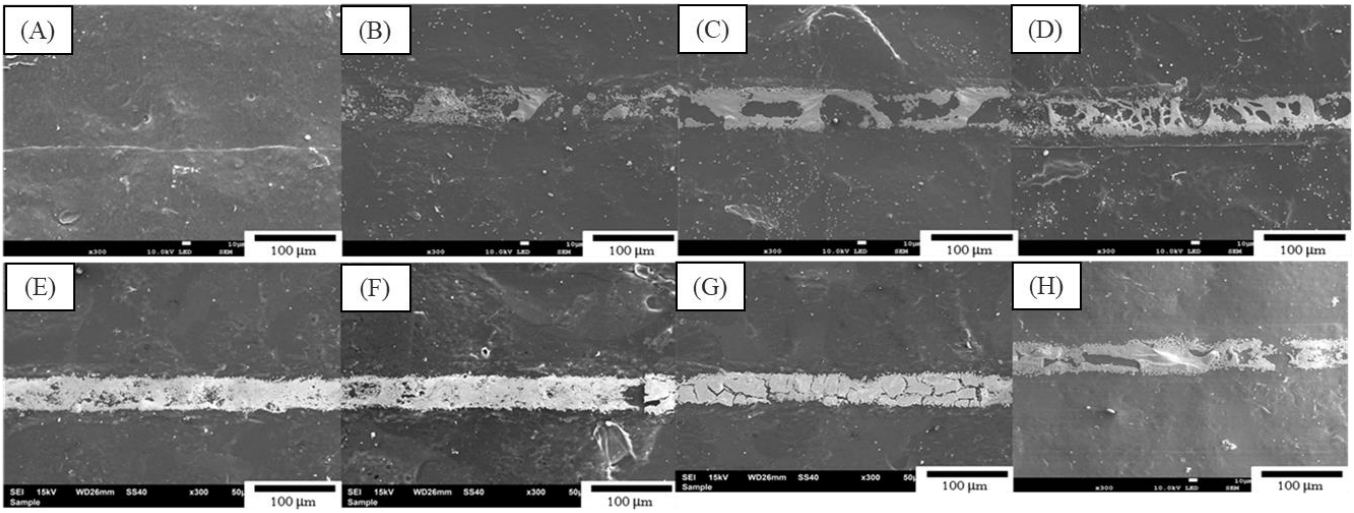

Figure 7. SEM images copper pattern after electroless deposition on duty cycle 40% at frequency 20 to 90 kHz (A) 20 kHz (B) 30 kHz (C) 40 kHz (D) 50 kHz (E) 60 kHz (F) 70 kHz (G) 80 kHz (H) 90 kHz.

3.2.2. The effect of different laser duty cycles on the electroless copper pattern

A superior metal coating layer can be produced by modifying the pulse energy which is applied to the Pd complex catalyst [34, 35]. Fig.8 (A) to (E) are SEM images of a PC/ABS substrate coated with ink after laser scanning at a frequency of 60 kHz in a duty cycle of 20% to 60%. Table 2 shows pulse energy density changes under different duty cycles. As shown in Fig. 10 (A) to (B), it can be observed that as the pulse energy density is greater than 1048 $\mu J/\mu m^2$, there is some defect in the middle of the line because the catalyst is oxidized by being overheated. As the duty cycle increase to 40% (pulse energy density decrease to 786 $\mu J/\mu m^2$), the center of the figure is less overheated, the copper metal line

is relatively complete (as shown Fig.8(C)). In Fig.8 (D) and Fig.8 (E), the duty cycle is higher than 50%, the pulse energy density is not enough and the reduction catalyst is less, the deposited copper metal is thinly, this phenomenon in the 60% condition of duty cycle is more obvious.

Table 2. The pulse energy density on frequency 60 kHz at different duty cycle (20 to 60%)

Input energy	Frequency (kHz)	Duty Cycle	Pulse energy density ($\mu J/\mu m^2$)
10%	60 kHz	20%	1572
		30%	1048
		40%	786
		50%	629
		60%	524

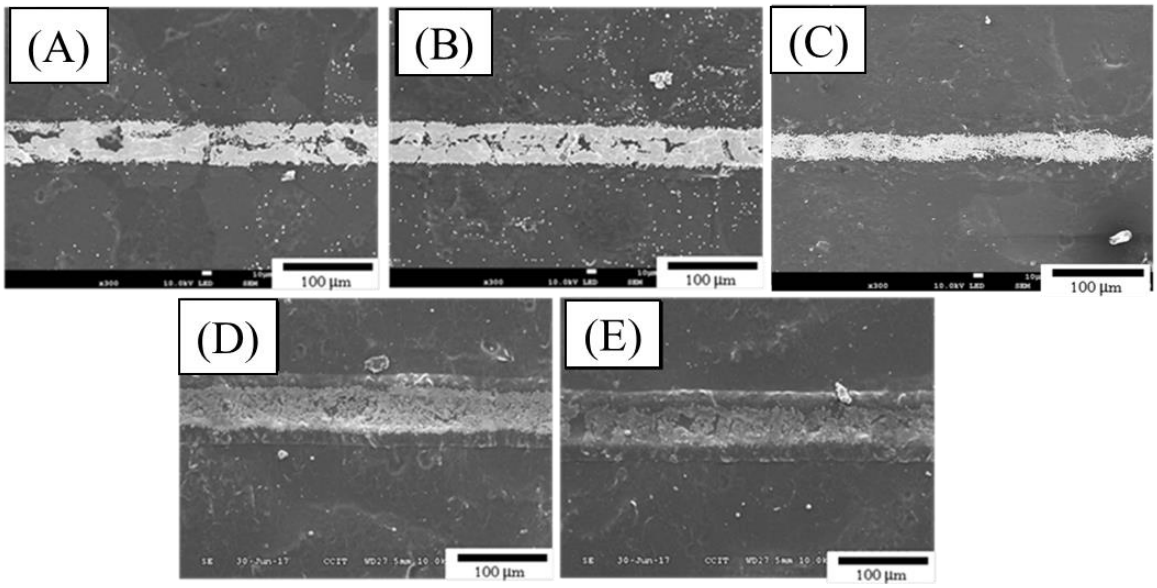

Figure 8. SEM images copper pattern of electroless deposition after laser scanning on frequency of 60 kHz at different duty cycles (A) 20% (B) 30% (C) 40% (D) 50% (E) 60%

We are apt to divide the duty cycle of 35% to 40% on 60 kHz into several parts to test. Table 3 shows pulse energy density changes under different duty cycles. Fig. 9 (A) to (C) shows SEM images of a PC/ABS substrate coated with Pd complex after laser scanning at a frequency of 60 kHz in a duty cycle of 35%, 37.5% and 40%. As shown in Fig.9 (A) to (C), it can be observed that as the pulse energy density is 933 $\mu J/\mu m^2$, the center of the circuit pattern cannot be plated well because the catalyst is oxidized by being overheated. Yet, when the pulse energy density is 878 $\mu J/\mu m^2$, the catalyst ions in the Pd complex can achieve a better reduction effect. Fig. 9 (B) shows that the copper metal has been deposited quite completely and intensively on the circuit pattern. In contrast, the pulse energy density with a duty cycle of 40% is small that sufficient catalyst cannot be produced completely, resulting in insufficient growth of the copper metal layer. From the above experimental results, it can be concluded that the best conditions are the frequency of 60 kHz, the duty cycle 37.5% pulse energy density of 878 $\mu J/\mu m^2$.

Table 3. The pulse energy density on frequency 60 kHz at different duty cycle (35 to 40%)

Input energy	Frequency (kHz)	Duty Cycle	Pulse energy density ($\mu J/\mu m^2$)
10%	60 kHz	35 %	933
		37.5 %	878
		40 %	786

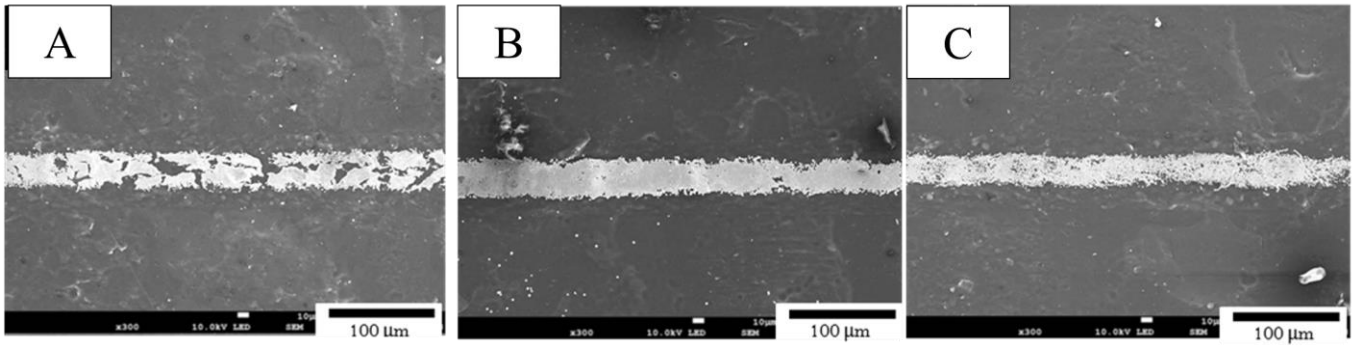

Figure 9. SEM image after laser scanning of 60 kHz at different duty cycles (A) 35% (B) 37.5% (C) 40%

3.2.3. The effect of different electroless copper parameter on the copper pattern

The temperature of electroless plating will affect the deposition of copper metal. In general, the higher the electroless plating temperature is, the stronger the driving force is [41]. Metal will be deposited quickly on the pattern at the initial stage of electroless plating since the driving force facilitate to form a moderate seed layer for copper metal autocatalysis. The SEM images of the copper layer deposited at different electroless plating temperatures are shown in Fig.10. The seed formed by the catalyst is ineffective because the driving force is low as the electroless plating temperature is 55°C, as shown in fig.10(A), A better effect of electroless plating will be achieved with rising temperature. Fig.10(C) displays that when the temperature is at 65°C, resulting in enough driving force to prompt the copper to be deposited on the pattern. Therefore, the electroless plating temperature of 65°C is the primary condition for preparing copper metal patterns, so that a complete and fine line width can be plated. Plating time is another factor that must be considered as well. It can be seen from Fig.11 that the variation in surface morphology of these copper layers suggests a definite dependence on electroless plating time. The surface morphology of SEM image demonstrates that the copper metal is deposited quite densely after 20 minutes of electroless plating.

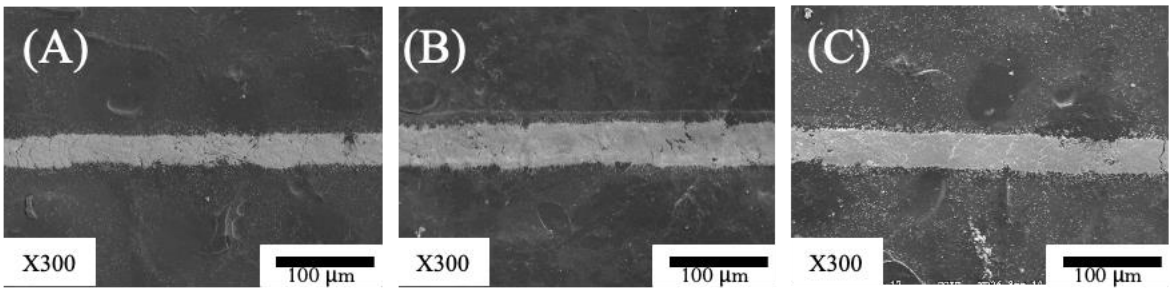

Figure 10. The electroless deposition temperature (A) 55℃ (B) 60 ℃ (C) 65 ℃

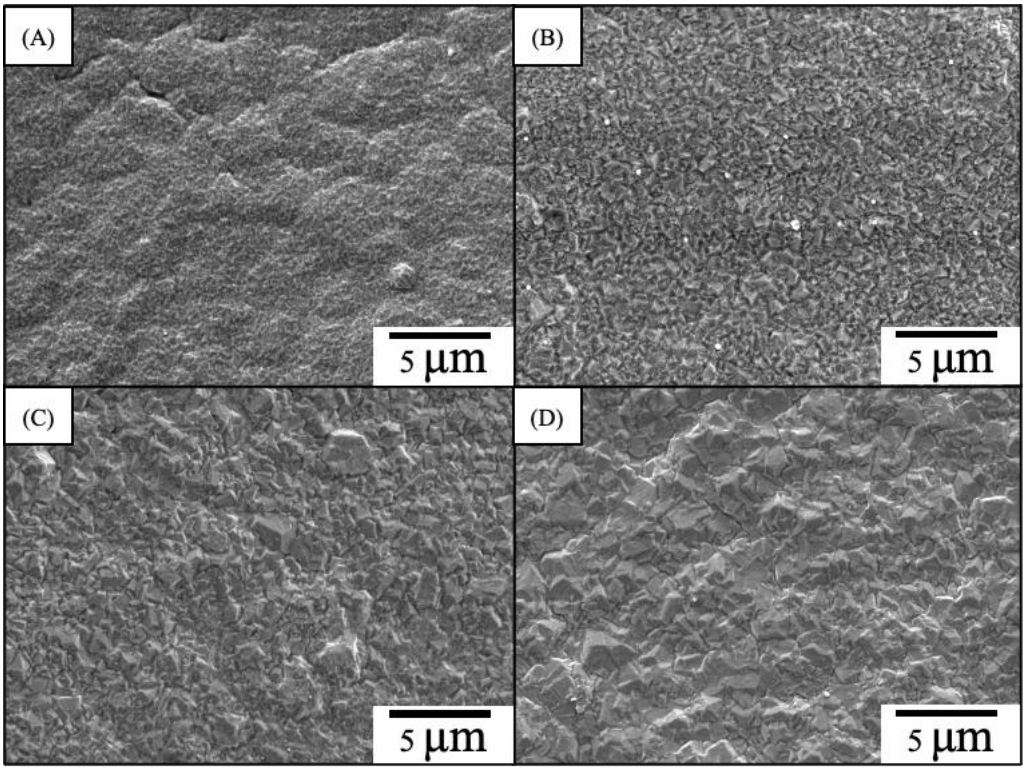

Figure 11. The SEM images of circuit surface topography at different times under 65℃ electroless plating conditions (A) 10 mins (B) 20 mins (C) 30 mins (D) 40 mins.

3.3 Application electronics circuit

The copper circuit pattern fabricated by the optimum parameters demonstrated excellent surface integrity after 3M 600 tape adhesion test. As shown in Fig 12(A)-(B), it is a circuit to test the circuit and apply to the metalized circuit during this research process. Fig 12(C) proves the conductivity of the precision circuit in this research. The resistance value of the sheet that was measured by a four-point probe is 0.125Ω/□. The laser activation treatment on the PC/ABS substrate is prone to obvious ablation, which can additionally improve the adhesion. [10, 36, 42, 43]. In this study, there is still great adhesion between the metal layer and the substrate in Figure 11. As shown in Fig.12(D) to (E), the superior

electrical conductivity of the copper circuiter the adhesion test by 3M 600 tape. The main reason is that the cross-linking molecules of 4VP and TMPTA can effectively enhance adhesion [37]. Therefore, our result indicates that the copper patterns on the PC/ABS substrate can be the prepared with ease by integration of laser-direct writing and electroless Cu plating.

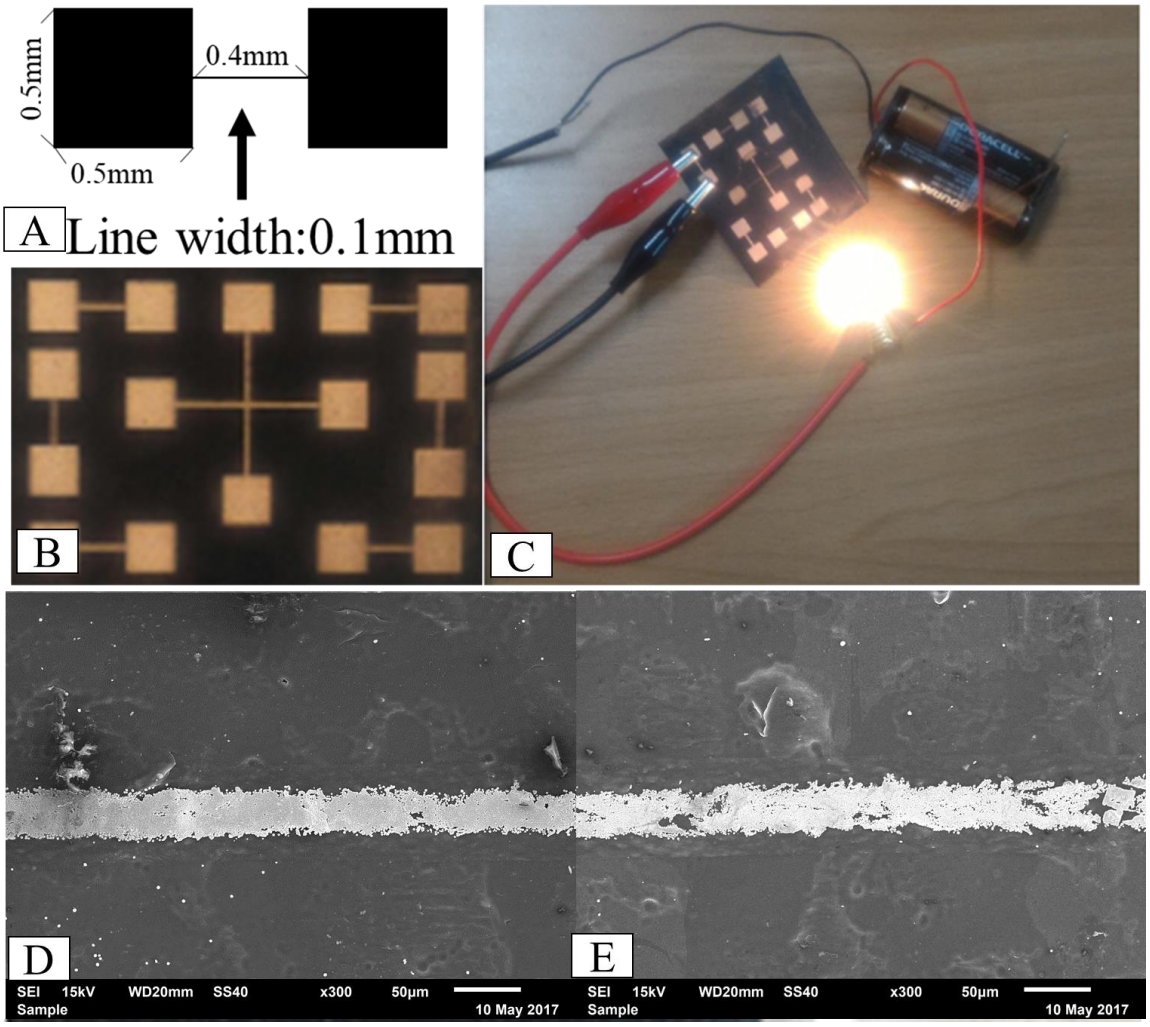

Figure 12. (A) Metallization graphic design (B) Activation through the best parameter selection, electroless copper metal circuit (C) PC/ABS circuits with working bulb light (D) Best parameters for copper-plated wire without electroplating parameters SEM (E) After 3M600 tape testing by SEM .

4. CONCLUSION

The copper metal pattern was successfully prepared by laser-assisted heating reduction of 4VP thermal cross-linking Pd complex and the thermal properties of palladium acetate were detected by TGA and DSC. After the temperature was higher than 220°C, palladium acetate was thermally cracked to

reduce palladium metal. Palladium oxide was produced as the temperature was higher than 440°C. ATR analysis showed that the peak at 1625 cm^{-1} for the Pd complex after the laser heating disappeared, which proved that the C=C bond was cross-linked and the XPS elemental analysis proved that the palladium metal after the laser was successfully reduced.

The optimal laser parameters are 10% input power, power density of 0.87 $mJ/\mu m^2$, frequency of 60 kHz, and duty cycle of 37.5%. The thermal accumulation effect is most suitable for 4VP thermal cross-linking on PC/ABS substrates. Type Pd complex, after laser heating, can be plated to complete a compact and continuous Cu line. The characteristics of low resistance, low roughness surface and excellent integrity of metal coating are used in a wider range of electronic circuits.

ACKNOWLEDGEMENTS
This work is sponsored by Ministry of Science and Technology of Taiwan under Grant No. MOST 106-2622-E-606-002 -CC2.

References

1. S.R. Forrest, *Nature*, 428 (2004) 911.
2. D.H. Kim, N. Lu, R. Ma, Y.S. Kim, R.H. Kim, S. Wang, J. Wu, S.M. Won, H. Tao, A. Islam, *Science*, 333 (2011) 838.
3. Y. Sun, J.A. Rogers, *Adv. Mater.*, 19 (2007) 1897.
4. Y. Jin, Y. Cheng, D. Deng, C. Jiang, T. Qi, D. Yang, F. Xiao, *ACS Appl. Mater. Interfaces*, 6 (2014) 1447.
5. D. Lee, D. Paeng, H.K. Park, C.P. Grigoropoulos, *ACS nano*, 8 (2014) 9807.
6. Y. Wang, H. Guo, J.J. Chen, E. Sowade, Y. Wang, K. Liang, K. Marcus, R.R. Baumann, Z.S. Feng, *ACS Appl. Mater. Interfaces*, 8 (2016) 26112.
7. G. Naundorf, H. Wissbrock, US Patent Application US7060421 B2 2006.
8. G. Naundorf, US Patent Application US20070247822 A1 2007.
9. G. Naundorf, WIPO Patent Application WO2007115546 A2 2006.
10. M. Hüske, J. Kickelhain, J. Müller, G. Eßer, *Proc.3rd LANE* 2001.
11. G. Naundorf, H. Wissbrock, *Galvanotechnik*, 91 (2000) 2449.
12. B.J. De Gans, P.C. Duineveld, U.S. Schubert, *Adv. Mater.*, 16 (2004) 203.
13. H. Yanagimoto, S. Deki, K. Akamatsu, K. Gotoh, *Thin Solid Films*, 491 (2005) 18.
14. A. Garcia, J. Polesel Maris, P. Viel, S. Palacin, T. Berthelot, *Adv. Funct. Mater.*, 21 (2011) 2096.
15. S. Ma, L. Liu, V. Bromberg, T.J. Singler, *ACS Appl. Mater. Interfaces*, 6 (2014) 19494.
16. S.P. Shen, W.P. Dow, *J. Electrochem. Soc.*, 161 (2014) D579.
17. H. Zhao, L. Hou, J. Wu, Y. Lu, *J. Mater. Chem. C*, 4 (2016) 7156.
18. S. Busato, A. Belloli, P. Ermanni, *Sens. Actuators, B*, 123 (2007) 840.
19. T. Zhang, X. Wang, T. Li, Q. Guo, J. Yang, *J. Mater. Chem. C*, 2 (2014) 286.
20. B. Yan, X. Huang, X. Song, L. Kang, Q. Le, K. Jiang, *J. Electrochem. Sci. Eng.*, 8 (2018) 331.
21. B.S. Cook, Y. Fang, S. Kim, T. Le, W.B. Goodwin, K.H. Sandhage, M.M. Tentzeris, *Electron. Mater. Lett.*, 9 (2013) 669.
22. A. Sridhar, J. Reiding, H. Adelaar, F. Achterhoek, D. Van Dijk, R. Akkerman, *J. Micromech. Microeng.*, 19 (2009) 085020.
23. Y. Chang, C. Yang, X.Y. Zheng, D.Y. Wang, Z.G. Yang, *ACS Appl. Mater. Interfaces*, 6 (2014) 768.
24. P.C. Wang, C.P. Chang, M.J. Youh, Y.M. Liu, C.M. Chu, M.D. Ger, *J. Taiwan Inst. Chem. Eng.*, 60 (2016) 555.

25. W. Xiong, Y.S. Zhou, W.J. Hou, L.J. Jiang, Y. Gao, L.S. Fan, L. Jiang, J.F. Silvain, Y.F. Lu, *Sci. Rep.*, 4 (2014) 1.
26. O. Azzaroni, Z. Zheng, Z. Yang, W.T. Huck, *Langmuir*, 22 (2006) 6730.
27. T. Kaufmann, B.J. Ravoo, *Polym. Chem.*, 1 (2010) 371.
28. J. Li, L. Liu, D. Zhang, D. Yang, J. Guo, J. Wei, *Synth. Met.*, 192 (2014) 15.
29. Y.Y. Nian, M.J. Youh, C.P. Chang, Y.C. Chen, M.D. Ger, *J. Taiwan Inst. Chem. Eng.*, 68 (2016) 423.
30. S.W. Suh, J.J. Kim, S.H. Kim, B.K. Park, *J. Ind. Eng. Chem.*, 18 (2012) 290.
31. D. Zabetakis, W.J. Dressick, *ACS Appl. Mater. Interfaces*, 4 (2012) 2358.
32. Y. Zhang, H.N. Hansen, A. De Grave, P.T. Tang, J.S. Nielsen, *Int. J. Adv. Manuf. Technol*. 55 (2011) 573.
33. K. Ratautas, M. Gedvilas, I. Stankevičiene, A. Jagminienė, E. Norkus, N.L. Pira, S. Sinopoli, U. Emanuele, G. Račiukaitis, *Proc. SPIE* 7 (2016) 9735.
34. S.-H. Lee, H. Yashiro, S.-Z. Kure-Chu, *Korean J. Mater. Res.*, 30 (2020) 327.
35. K. Ratautas, A. Jagminienė, I. Stankevičienė, M. Sadauskas, E. Norkus, G. Račiukaitis, *Results Phys.*, 16 (2020) 102943.
36. K. Ratautas, V. Vosylius, A. Jagminienė, I. Stankevičienė, E. Norkus, G. Račiukaitis, *Polymers*, 12 (2020) 2427.
37. K. Ratautas, M. Gedvilas, I. Stankevičiene, A. Jagminienė, E. Norkus, N.L. Pira, S. Sinopoli, G. Račiukaitis, *Appl. Surf. Sci.*, 412 (2017) 319.
38. P. Rytlewski, B. Jagodziński, T. Karasiewicz, P. Augustyn, D. Kaczor, R. Malinowski, K. Szabliński, M. Mazurkiewicz, K. Moraczewski, *Materials*, 13 (2020) 2224.
39. P.C. Wang, Y.M. Liu, C.P. Chang, Y.Y. Liao, Y.Y. Peng, M.D. Ger, *J. Taiwan Inst. Chem. Eng.*, 80 (2017) 963.
40. C. Zhu, Y. Li, X. Liu, *Polymers*, 10 (2018) 573.
41. S.-A. Xu, C.-S. Liang, *Int. J. Electrochem. Sci.*, 11 (2016) 8817.
42. J. Zhang, T. Zhou, Y. Xie, L. Wen, *Adv. Mater. Interfaces*, 4 (2017) 1700937.
43. K. Ratautas, M. Gedvilas, I. Stankevičiene, A. Jagminienė, E. Norkus, *Sci. Rep.* 6 (2016) 22963.